International Journal of Orthopaedics

Online Submissions: http: //www.ghrnet.org/index.php/ijo
doi: 10.17554/j.issn.2311-5106.2023.10.485

Int. J. of Orth. 2023 June 28; **10(2)**: 1735-1742
ISSN 2311-5106 (Print), ISSN 2313-1462 (Online)

ORIGINAL ARTICLE

Biomechanical Analysis of Damage Formation in Total Hip Arthroplasty under Falling Conditions

Aiman Izmin[1], Mitsugu Todo[1,2], Takuaki Yamamoto[3]

1 Interdisciplinary Graduate School of Engineering Sciences, Kyushu University, 6-1 Kasuga-koen, Kasuga, Fukuoka 816-8580, Japan;
2 Research Institute for Applied Mechanics, Kyushu University, 6-1 Kasuga-koen, Kasuga, Fukuoka 816-8580, Japan;
3 Department of Orthopedic Surgery, Faculty of Medicine, Fukuoka University, 7-45-1 Nanakuma, Jonan-ku, Fukuoka 814-0180, Japan.

Conflict-of-interest statement: The author(s) declare(s) that there is no conflict of interest regarding the publication of this paper.

Open-Access: This article is an open-access article which was selected by an in-house editor and fully peer-reviewed by external reviewers. It is distributed in accordance with the Creative Commons Attribution Non Commercial (CC BY-NC 4.0) license, which permits others to distribute, remix, adapt, build upon this work non-commercially, and license their derivative works on different terms, provided the original work is properly cited and the use is non-commercial. See: http://creativecommons.org/licenses/by-nc/4.0/

Correspondence to: Mitsugu Todo, Interdisciplinary Graduate School of Engineering Sciences, Kyushu University, 6-1 Kasuga-koen, Kasuga, Fukuoka 816-8580, Japan.
Telephone: +81-92-583-7762
Email: todo@riam.kyushu-u.ac.jp

Received: May 26, 2023
Revised: June 10, 2023
Accepted: June 13 2023
Published online: June 28, 2023

ABSTRACT

Computational finite element models of femoral bones, bone X and Y, with different bone quality were constructed using CT-images of two elderly female patients. Then, three different stem models of total hip arthroplasty (THA) were implanted into the femoral models. Nonlinear finite element analysis was performed under four different falling conditions in order to assess the effects of bone quality and stem design on the fracture mechanisms of femoral bone. It was found that the stem geometry had some effects on the cumulative number of element failures in the internal region of bone X (greater bone quality) along with the changes in the falling condition, while such effects were very small in bone Y models with lower bone quality. By analyzing the damage formation in the external bone regions, it was found that the fracture formation drew a parallel view to type A_G of Vancouver fracture classification which occurred in all of the THA models. It was also found that the internal damage distribution of the THA models of bone X had a pattern of concentrated damages at zone 1 and zone 7 of the Gruen zone system and the pattern was consistent in all stem designs and falling conditions. On the contrary, in the THA models of bone Y, the damaged distributions were scattered throughout the bone-stem interfaces.

Key words: Total hip arthroplasty; Finite element method; Bone quality; Implant design; Bone fracture

© 2023 The Author(s). Published by ACT Publishing Group Ltd. All rights reserved.

Izmin A, Todo M, Yamamoto T. Biomechanical Analysis of Damage Formation in Total Hip Arthroplasty under Falling Conditions. *International Journal of Orthopaedics* 2023; **10(2)**: 1735-1742 Available from: URL: http://www.ghrnet.org/index.php/ijo/article/view/3377

INTRODUCTION

Over the years, total hip arthroplasty (THA) has been known to be one of the standard treatments for severe hip diseases to improve the patient's quality of life and afford reliable long-term pain relief[1,2]. It has been reported that patients with hip diseases usually experience physical problems such as gait disorder and instability which have a correlation with the number of falls incident in the preceding year[3,4]. Despite the success in reducing hip pain after THA, falling after the surgery might be even riskier. The most critical period is said to be within a year after the surgery in which 30 % to 40 % of cases fell at least once and some of them were hospitalized due to serious injuries, i.e., bone fracture[5,6]. Several studies reported that the cause of falls after THA was due to gait abnormality and muscle weakness[7,8]. Since the possibility of this traumatic incident is likely to happen to

any patient after undergoing THA, the mechanisms of bone fracture under falling conditions after THA must be well understood to prevent such incident.

Several studies were conducted to determine the impact of falling on the mechanical behavior of femurs by experimental and finite element analysis[9,10] and however, only a few studies were performed to investigate the impact on the femurs with THA under the falling conditions. For example, Franceschini et al., conducted a computational study on different stem designs to predict the stress distribution in the homogeneous FE femoral bone model[11]. They found that the distribution of stress was greatly affected by the stem design in the bone under the falling conditions. From the mechanical point of view, bone quality also plays an important role in determining the impact of falling conditions where poor bone quality, e.g., low bone mineral density might result in high severity of damage[12]. Introduction of inhomogeneous FE bone models with distributed mechanical properties may be helpful to predict the effects of falling conditions on the mechanical performances of implanted bones with different quality.

In this study, previously, two femoral bone models with different bone quality were developed from CT images of two female patients[13]. Three different stem models of THA were then implanted into the bone models and their FE models were analyzed using nonlinear theories under four different falling conditions. Effects of bone quality, stem design and falling condition on the femoral damage mechanism were then investigated.

ANALYSIS METHOD

Modeling of femoral bones

Computed tomography (CT) images of two patients with the slice thicknesses of 0.5 mm were used in this analysis. Both patients are female and diagnosed with stage three of avascular necrosis on the right femur. One patient has an age of 61, while another is 87 years old. In this study, the FE model from the 61 and 87-year-old patients were labeled with bone X and Y, respectively. Their CT images in DICOM format were compiled using the bone analysis software, Mechanical Finder version 11 (Research Center for Computational Mechanics, Tokyo, Japan). The region of interest (ROI) was thoroughly selected from the CT images, and those images were vertically stacked to construct a three-dimensional (3D) geometry of the femur. The trabecular and internal cortical bones were meshed with 2-mm tetrahedral solid elements and the outer cortical surface was covered with 2-mm triangular plate shell elements.

The elastic modulus and the compressive yield stress were calculated in every element using the proposed equations by Keyak et al., and Keller[14,15] and the average bone mineral density (BMD) of the element. The BMD values were determined from the linear relationship with the CT values in Hounsfield Unit (HU). The Poisson's ratio was set to 0.4[14]. The mechanical properties of the outer cortical shell elements were set to be the same with the adjacent solid element under its location.

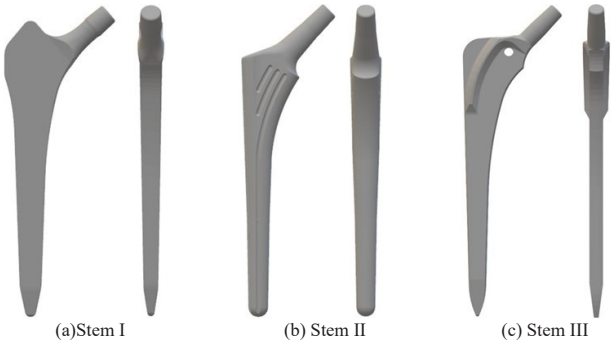

Figure 1 Illustrations of three stem models.

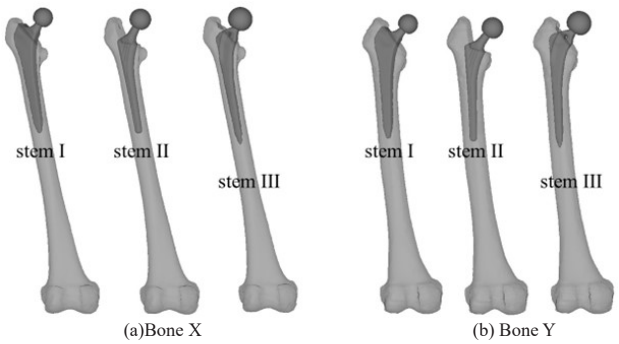

Figure 2 THA models constructed by combining a femoral model and a stem.

Construction of THA models

Three types of stems with different designs were implanted into bone X and Y as shown in Figure 1. Those stems were labeled with stem I, stem II, and stem III. The femoral osteotomy was applied at the proximal region of the femur and the implant was carefully placed

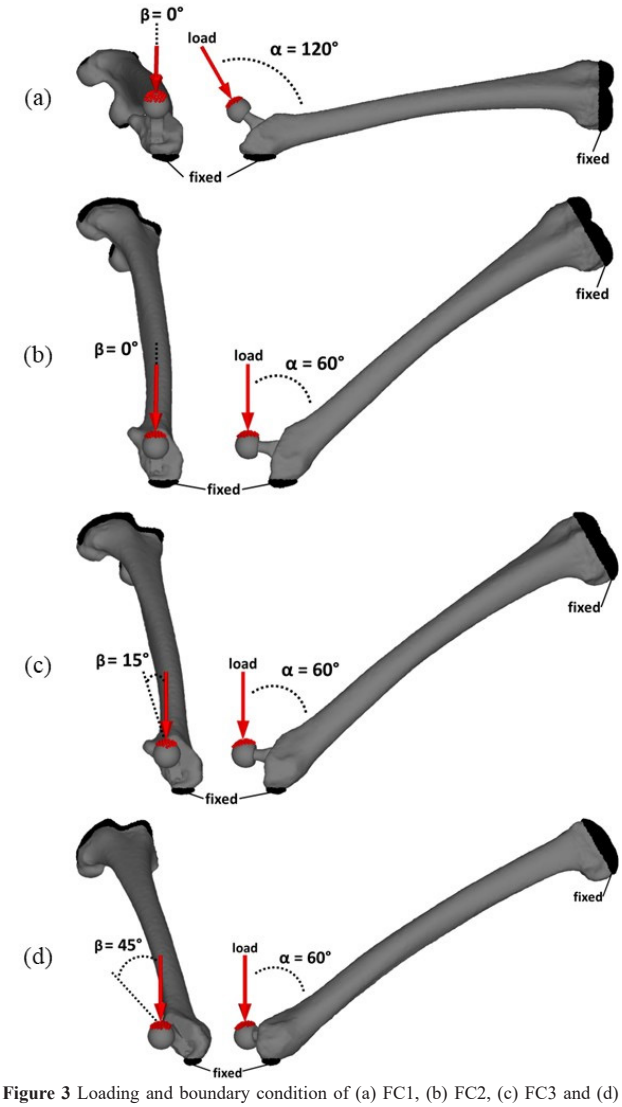

Figure 3 Loading and boundary condition of (a) FC1, (b) FC2, (c) FC3 and (d) FC4.

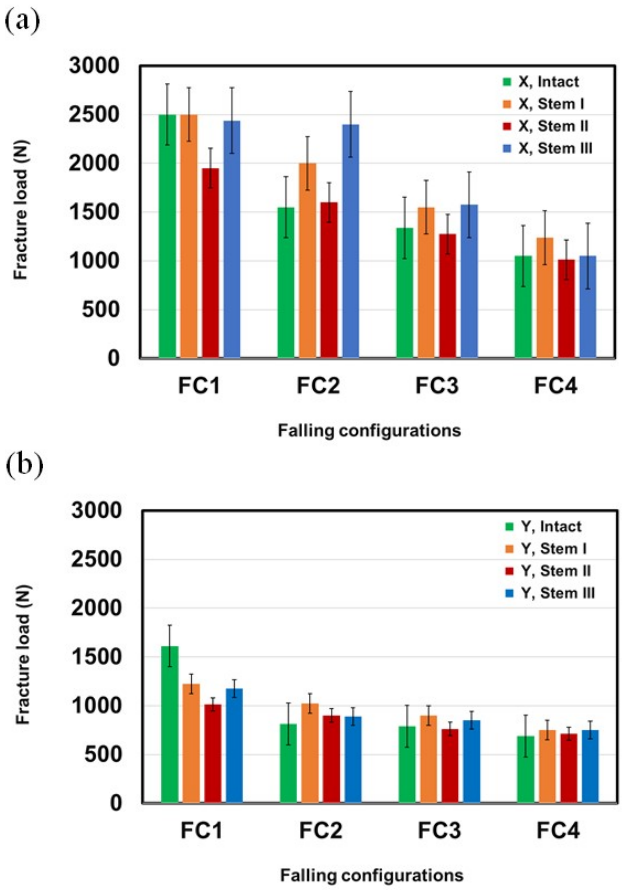

Figure 4 Fracture load of intact and THA models of (a) bone X and (b) bone Y.

inside the femoral canal. The osteotomy was conducted considering the vertical height and medial offset of the stem to ensure the proximal area of the stem was appropriately placed at the center of rotation of the original hip. The THA models are illustrated in Figure 2. The total numbers of elements in the finite element THA models with bone X and stem I, stem II, and stem III were 162,710, 155,220, 139,579 of solid elements, and 62,628, 61,533, 62,547 of shell elements, respectively. For bone Y, the total numbers of elements in THA models with stem I, stem II, and stem III were 189,777, 185,391, 175,221 of solid elements and 74,766, 74,190, 75,165 of shell elements, respectively.

The femoral components of the implant, i.e., femoral ball and stem, were assigned with the properties of titanium alloy (E=114 GPa, v=0.34) and alumina ceramic (E=370 GPa, v =0.22), respectively [16]. The element between the bone and the stem interfaces were designed to be perfectly bonded. The material properties of bones were determined by using Keyak and Keller's equations as explained in the previous section.

Boundary conditions

Four different types of falling conditions were adopted from the previous studies[9]. Those conditions were labeled with FC1, FC2, FC3, and FC4. Each falling condition has different angles of α and β to mimic the real situation of falling onto the lateral side and posterolateral side of the femur. All falling conditions are shown in Figure 3. A stepwise load from 0 N to 2500 N in 20 steps with 125 N load increment was applied to all models in each condition. The maximum loading magnitude, i.e., 2500 N was determined from previous study which was sufficient to demonstrate bone fracture at the outer cortical region of the femur.

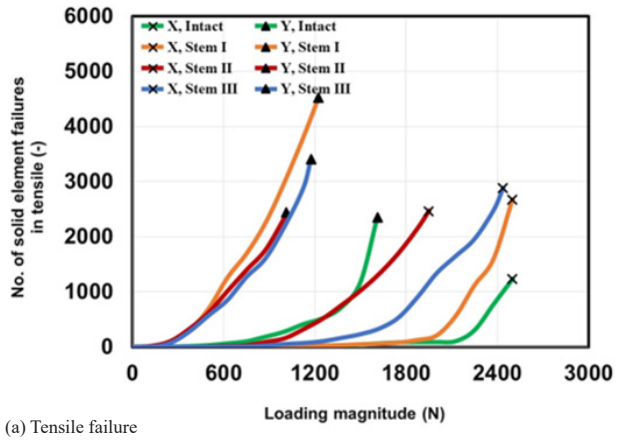

(a) Tensile failure

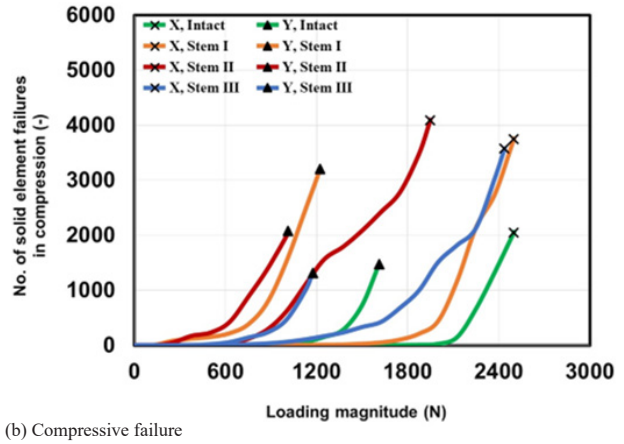

(b) Compressive failure

Figure 5 Number of solid element failures under FC1 condition.

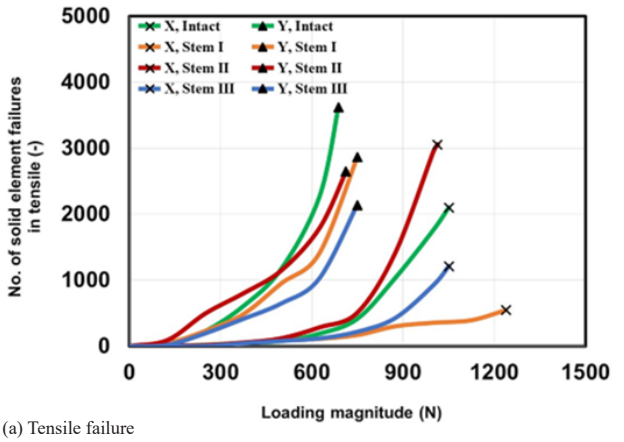

(a) Tensile failure

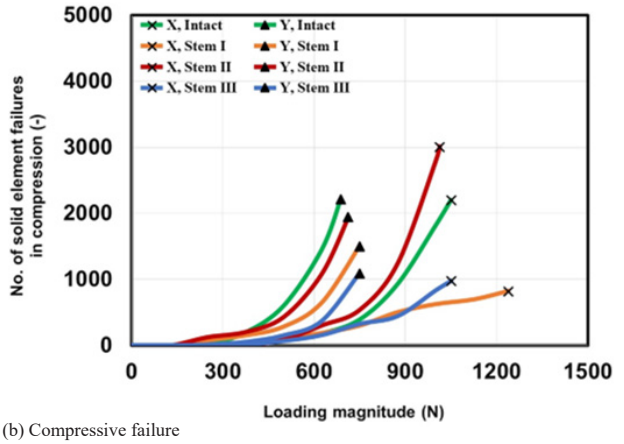

(b) Compressive failure

Figure 6 Number of solid element failures under FC4 condition

Mechanical theories for bone

The deformation behaviors of the bone elements were assumed to be bi-linear elastoplastic under compressive stress and linear elastic under tensile stress conditions. The work hardening rate for the compressive elastoplastic model was set to 0.05. The onset of plastic deformation was assessed using the Drucker-Prager yield criterion with use of the compressive yield strength which was determined by Keyak and Keller equations for each element[17,19]. Then, the compressive fracture of plastically deformed elements was assumed to take place when the minimum principal strain reached its critical value of -3000μ. On the contrary, the tensile fracture of elements was assumed to occur when the maximum principal stress reached its critical value which was equal to 0.8 times the compressive yield strength. In this study, the fracture load of bone was defined as a critical load at which 300 elements were failed under tensile or compressive stress state.

RESULTS AND DISCUSSION

Comparison of Fracture load

The fracture load values of the intact and THA models with bone X and Y under all falling conditions are shown in Figure 4. It was clearly seen that FC1 had the highest fracture load compared to the others. In addition, it was found that different THA designs produced different fracture loads to both the bone X and Y, especially stem II exhibited the lowest fracture load. The bone X possessed greater fracture loads for all conditions than the bone Y as a result of greater bone quality. It was also interesting to see that the intact bone models exhibited the highest fracture load under FC1, while the lowest fracture load was observed in the intact models under FC4.

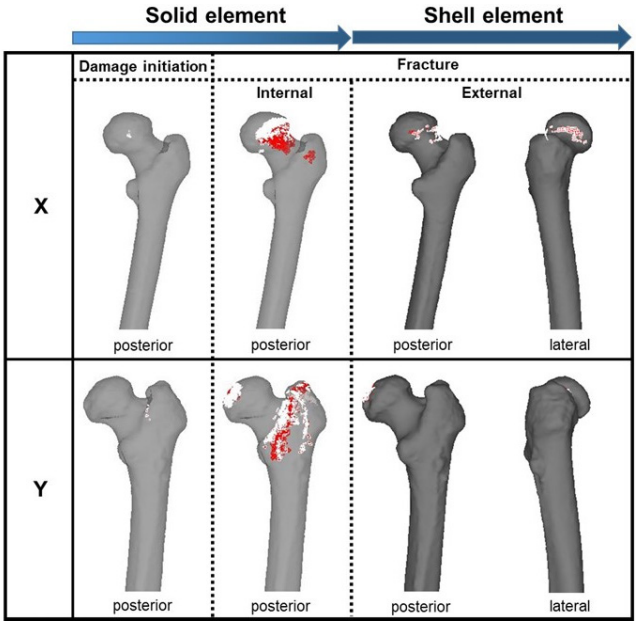

(a) Intact model

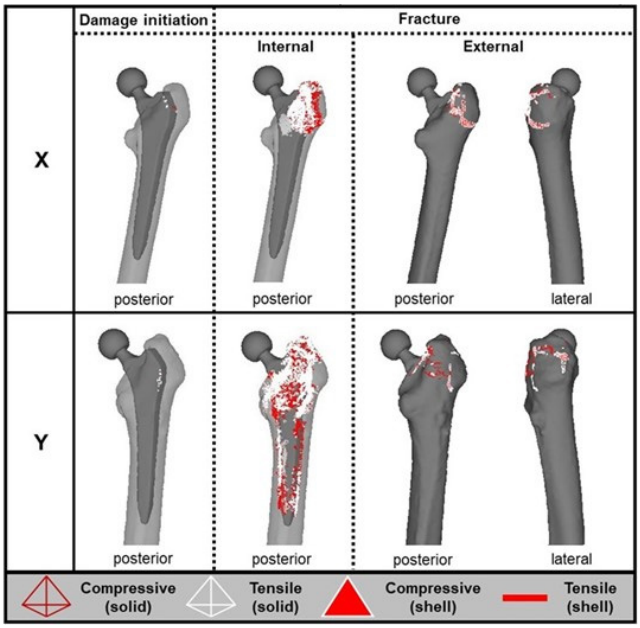

(b) Stem I model

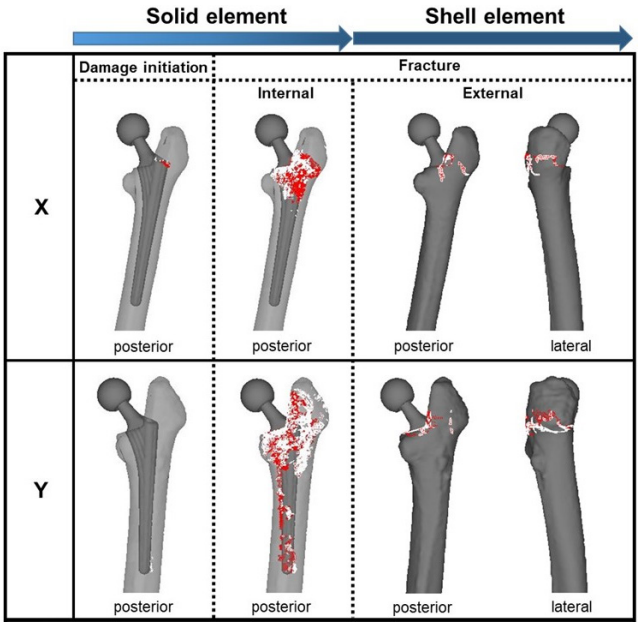

(c) Stem II model

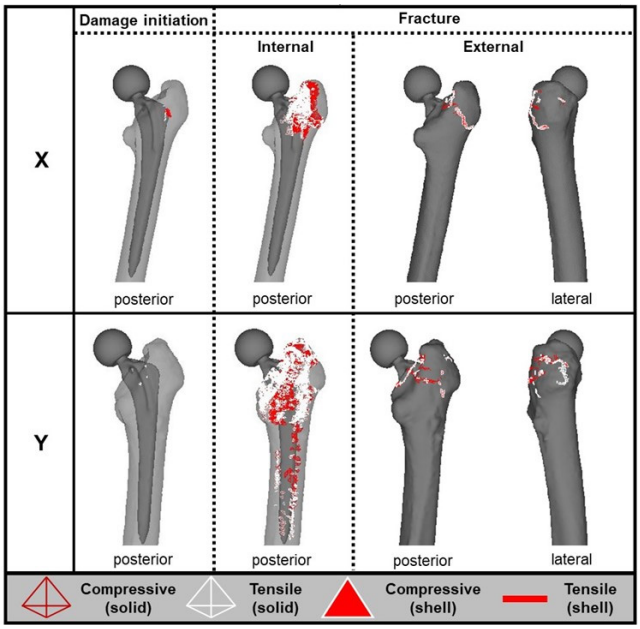

(d) Stem III model

Figure 7 Distribution of solid and shell element failures under FC1.

Accumulation of element failures

The cumulative numbers of solid element failures of bone X and bone Y under FC1 and FC4 are shown in Figures 5 and 6, respectively. Figure (a) and (b) exhibit the tensile failures and the compressive failures, respectively. It was observed that the compressive failures were dominant for bone X, while the tensile failures were dominant for bone Y. This pattern was consistent in all FCs. The cumulative number of solid element failures tended to gradually increase in the beginning and then rapidly increase until the fracture load in all FCs. The stem design obviously influenced the element failure behavior especially to the bone X. The main difference of element failure behavior between the stem designs implanted in bone X was the increasing gap as the falling condition shifted from lateral to posterolateral side. For bone Y, the effect of stem design on the element failure behavior was found to be small.

Under the condition of falling onto the lateral side such as FC1, the design of stem II tended to degrade the fracture load level of bone X, while the differences of the fracture load level were found to be small under the condition of FC4. For bone Y, the fracture load level showed no significant differences between all models in all FCs, except for FC1, where the intact femur model had slightly higher fracture load. In addition, it was clearly seen that the fracture load value of bone X was much higher than that of bone Y for both intact and stem insertion models, suggesting that bone X was much stronger than bone Y, under these falling configurations.

Micro-damage distribution in bone

Distribution of element failures under FC1 and FC4 are shown in Figures 7 and 8, respectively. The damaged solid elements expressed the distribution of internal micro-damages of bone at both the initial and final stages of fracture, while the damaged shell elements indicated the distribution of external micro-damages of the outer

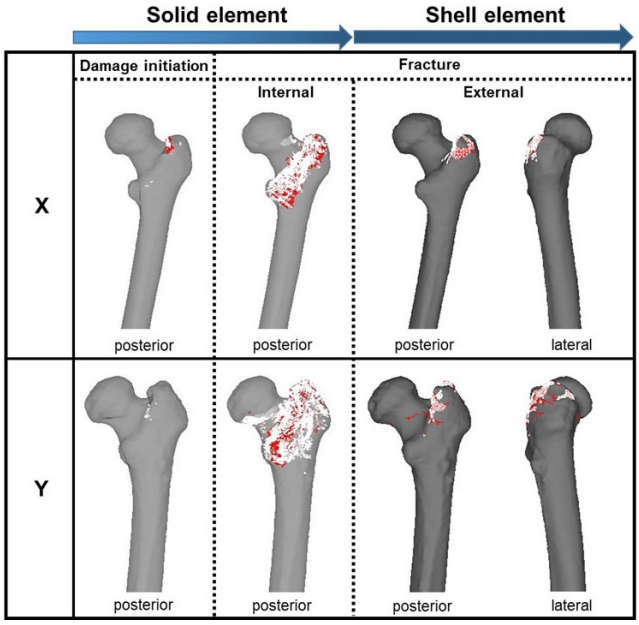

(a) Intact model

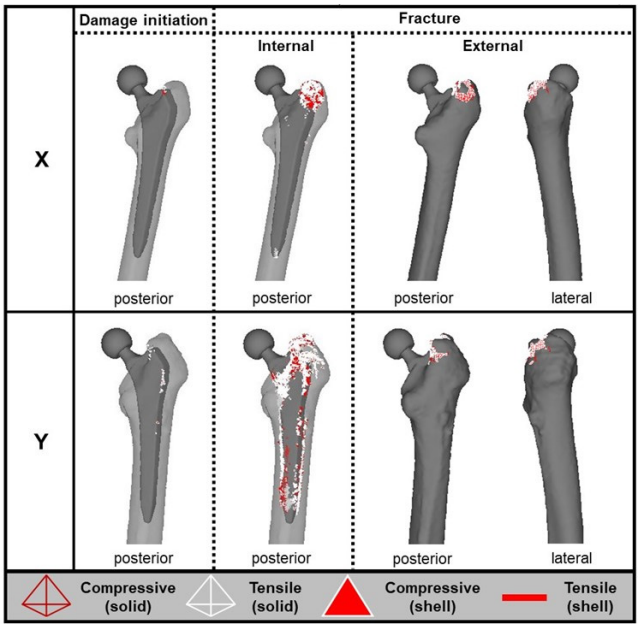

(b) Stem I model

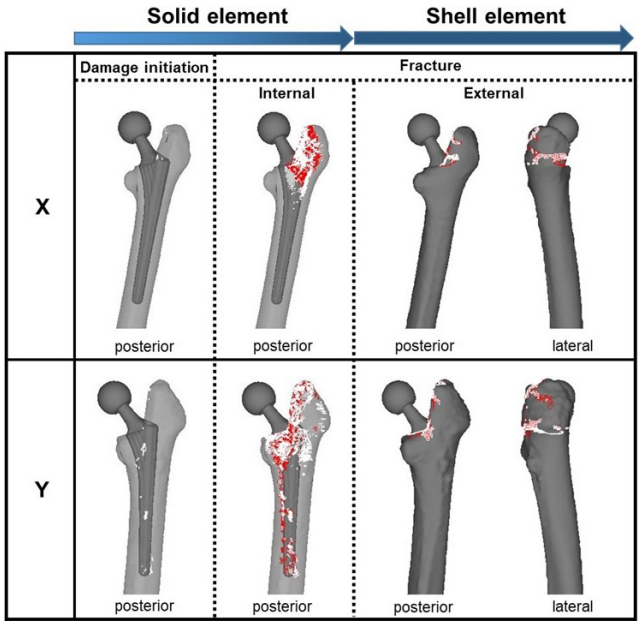

(c) Stem II model

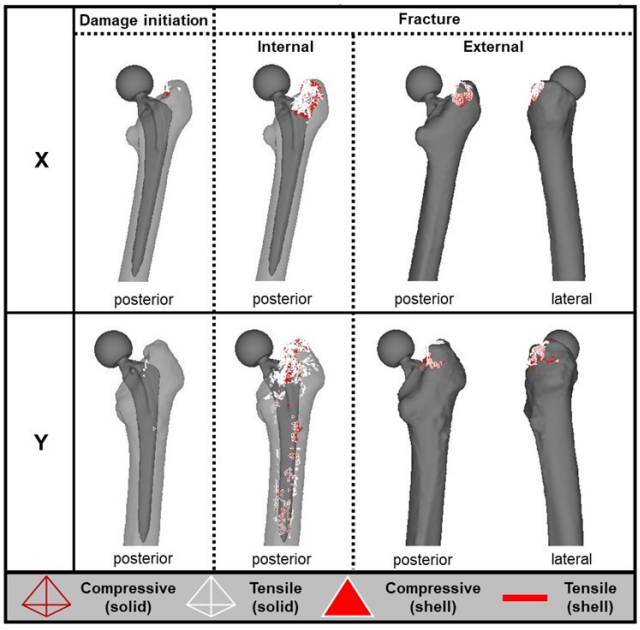

(d) Stem III model

Figure 8 Distribution of solid and shell element failures under FC4.

surfaces at the final stage of fracture.

It was observed that the initial damages were concentrated in the region close to the shoulder of the THA stem in bone X under all FCs, despite having different implant designs. However, for the case of bone Y, it was found that the initial damages were concentrated in different regions close to the stem shoulder, distal end, and flanges under FC1. On the other hand, under FC4, the damage initiation was seen to be scattered at several locations along the stems.

At the fracture stage, it was found that the micro-damage formation occurred at the trochanteric region in all the THA models of both bone X and bone Y. This type of fracture mode drew a parallel view to type A_G in the Vancouver Classification of periprosthetic fracture[20]. The fracture locations were similar under all FCs. Despite having similar fracture patterns and locations, bone Y models exhibited greater damage distributions in the internal regions. This could be observed in the internal view of the bone after the outer cortical shell fractured. The damaged elements were distributed throughout the bone-stem interface of bone Y, while the damages in bone X models were concentrated mostly in the shoulder area of the implant, resulting from the impact of falling onto the trochanteric region of the femur.

Internal damage distribution

Further analysis on the internal damage distribution was conducted by extracting the number of damaged elements based on the Gruen zone system. The extraction sizes of zones 1, 2, 4, 6, and 7 were similar in all stems, while the extraction sizes of zones 3 and 5 were differ and depending on the length of the stem. The results of the analysis are presented in Figures 9 and 10 for bone X and Y, respectively.

Most of the damaged elements were seen to be concentrated in zones 1 and 7 for bone X despite being implanted with different stem designs. The pattern was seen to be consistent in every FCs. The concentrated damaged elements at zones 1 and 7 were thought to be the result of the high impact loading exerted onto the trochanteric region of the femur. In zone 1, the damaged elements were dominated by the compressive element failures labeled in red color, whereas, in zone 7, the tensile element failures (white color) were dominant. The surrounding bones at the shoulder of the stem are considered to absorb most of the compressive impact during falling, while the bones attached to the medial side of the stem might be stretched away. This kind of mechanical behavior was expected since the elements constructing the bone-stem interfaces were designed to be perfectly bonded to mimic the complete process of the osseointegration between the bone and the stem.

A different scenario was observed in bone Y. It could be seen that the damaged elements were scattered throughout the zones, except for zone 4. The pattern was seen to be consistent in all of the THA models and FCs. Based on the result, the damaged elements were almost comparable between the lateral side of the bone-stem interface (zone 1, 2, 3) and the zones at the medial side (zone 5, 6, 7). At the proximal region of the implant stem, the bones at zone 1

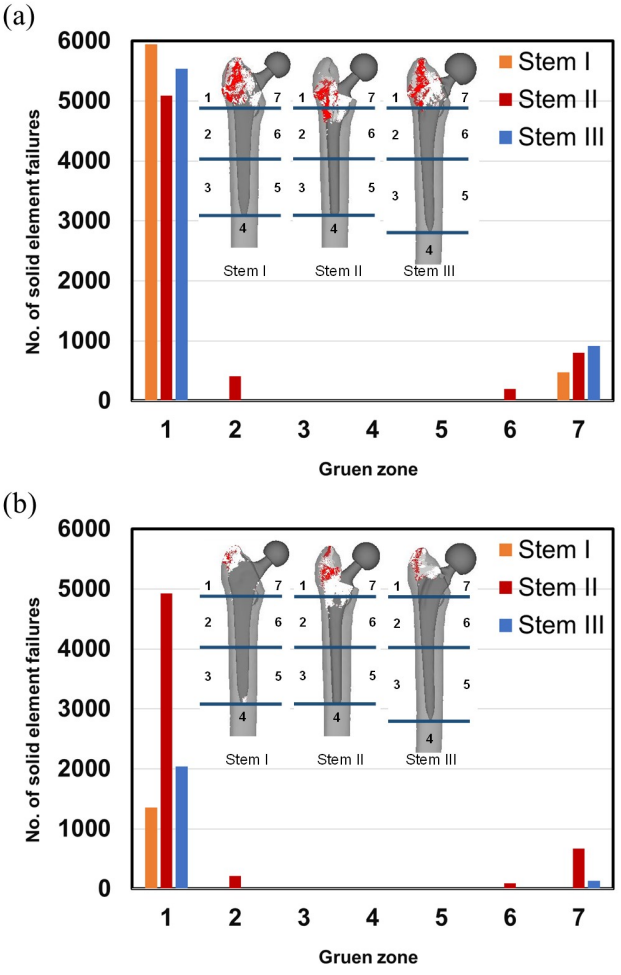

Figure 9 Internal damage distribution on THA models of bone X: (a) FC1, (b) FC4.

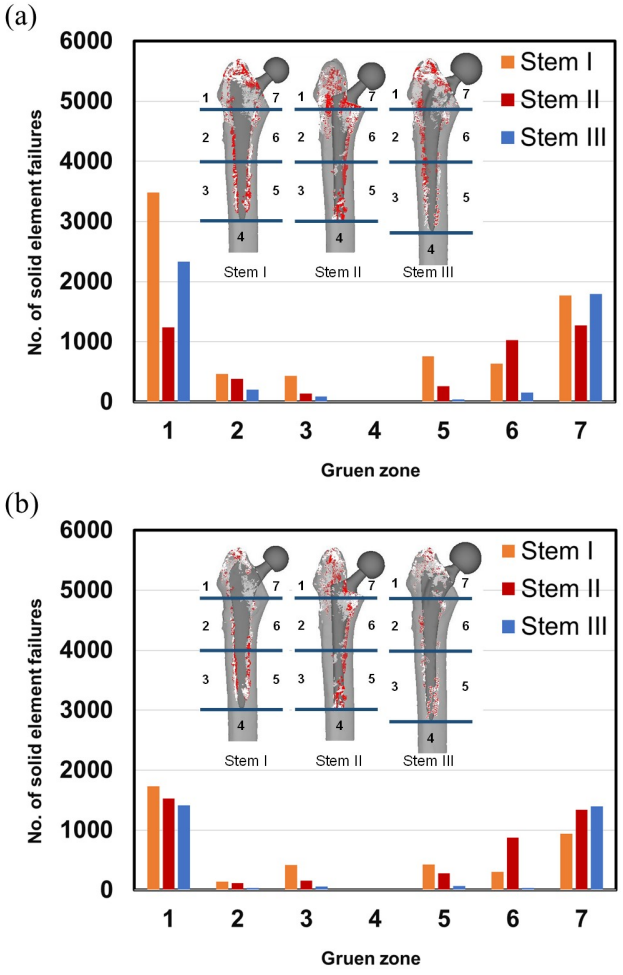

Figure 10 Internal damage distribution on THA models of bone Y: (a) FC1, (b) FC4.

were thought to experience severe damage compared to zone 7. In the middle region of the implant stem, bone damages in zone 6 were slightly higher than those in zone 2. At the distal end region of the implant stem, bones at zone 5 experienced slightly higher damages than zone 3. This pattern was consistent at THA models of bone Y in all FCs.

In addition, it was found that the tensile element failures were dominant in most of the zones. It is considered that there are two possibilities behind this phenomenon. First is the factor of poor bone quality. Poor bone quality corresponds to lower bone stiffness, and such bones with lower stiffness may easily break, if the applied forces exceed their ultimate tensile strength values. The second reason for this phenomenon may be due to the size of the stems which do not perfectly fit into bone Y. If a stem does not perfectly fit in the proximal region of femur, the force exerted onto the femoral ball will produce a bending moment, causing a bending effect to the stem which may damage the bones in the regions along the stem. As supporting evidence, most of the bone elements failed under compression were noticed to accumulate in the middle and distal area of the stems which can be seen in zone 2-3 and 5-6 of bone Y, as a result of the bending effect from the stem.

CONCLUSIONS

Two femoral bones with different quality, namely, bone X and bone Y were successfully developed using CT-images of two elderly female patients. Three types of THA stem with different designs were then implanted into the femoral models. Four different kinds of falling condition, FC1, FC2, FC3, and FC4, were adopted as the boundary condition for FEA to assess the fracture mechanisms of the femurs when falling down by different sides, such as lateral and posterolateral. The fracture load was found to be reduced with the change of falling condition, resulting from the different degrees of falling. A formation of concentrated damaged elements was observed in the THA models of bone X in both the initiation and fracture stages from the internal view. On the contrary, bone Y showed a scattered formation of damaged elements with stem II under FC4 during the initiation stage. Such scattered formation was also observed with all stems and FCs of bone Y at the stage of fracture. In the external region, the damaged elements were found to be located in the trochanteric region in all of the THA models with different fracture severity determined based on the number of shell element failures. Based on the Gruen zone system, only two zones (1 and 7) were found to be the most vulnerable area with the extensive formation of damaged elements for THA models of bone X, while for bone Y, the damaged elements were comparable between the lateral side (zone 1, 2, 3) and medial side (zone 5, 6, 7) of the bone-stem interface resulting from its poor bone quality. This study clearly indicated that the nonlinear CT-FEM could be useful to fully investigate the effects of bone quality and implant design on the fracture mechanisms of femoral bones. The FEA results will be used to solve the problems related to THA complications and bone fracture prevention in the future.

REFERENCES

1 L. Shan, B. Shan, D. Graham, and A. Saxena, "Total hip replacement: A systematic review and meta-analysis on mid-term quality of life," *Osteoarthr. Cartil.*, 2014 Mar; 22(3): 389-406. [PMID: 24389057]; [DOI: 10.1016/j.joca.2013.12.006]

2 G. G. Polkowski, J. J. Callaghan, M. A. Mont, and J. C. Clohisy, "Total hip arthroplasty in the very young patient," *J. Am. Acad. Orthop. Surg.*, 2012 Aug; 20(8): 487-97. [PMID: 22855851]; [DOI: 10.5435/JAAOS-20-08-487]

3 O. Wada, T. Asai, Y. Hiyama, S. Nitta, and K. Mizuno, "Gait Variability in Women with Hip Osteoarthritis before and after Total Hip Replacement: A Prospective Cohort Study," *Am. J. Phys. Med. Rehabil.*, 2019 Oct; 98(10): 866-871. [PMID: 31045874]; [DOI: 10.1097/PHM.0000000000001206]

4 W. F. Peter *et al.*, "The association between comorbidities and pain, physical function and quality of life following hip and knee arthroplasty," *Rheumatol. Int.*, 2015 Jul; 35(7): 1233-41. [PMID: 25586654]; [PMCID: PMC4436688]; [DOI: 10.1007/s00296-015-3211-7]

5 H. Ikutomo, K. Nagai, N. Nakagawa, and K. Masuhara, "Falls in patients after total hip arthroplasty in Japan," *J. Orthop. Sci.*, 2015 Jul; 20(4): 663-8. [PMID: 25797333]; [DOI: 10.1007/s00776-015-0715-7]

6 P. Levinger, E. Wee, S. Margelis, H. B. Menz, J. R. Bartlett, N. R. Bergman, S. McMahon, and K. D. Hill, "Pre-operative predictors of post-operative falls in people undergoing total hip and knee replacement surgery: a prospective study," *Arch. Orthop. Trauma Surg.*, 2017 Aug; 137(8): 1025-1033. [PMID: 28597247]; [DOI: 10.1007/s00402-017-2727-6]

7 H. Ikutomo, K. Nagai, K. Tagomori, N. Miura, N. Nakagawa, and K. Masuhara, "Gait Abnormality Predicts Falls in Women After Total Hip Arthroplasty," *J. Arthroplasty*, 2018 Oct; 33(10): 3215-3219. [PMID: 29941382]; [DOI: 10.1016/j.arth.2018.05.044]

8 X. Bin Lin, W. H. Wu, R. H. A. Weijer, M. R. Prins, J. H. van Dieën, S. M. Bruijn, and O. G. Meijer, "Strong relationship of muscle force and fall efficacy, but not of gait kinematics, with number of falls in the year after Total Hip Arthroplasty for osteoarthritis: An exploratory study," *Clin. Biomech.*,2022 Feb; 92: 105551. [PMID: 34998081]; [DOI: 10.1016/j.clinbiomech.2021.105551]

9 M. Bessho, I. Ohnishi, T. Matsumoto, S. Ohashi, J. Matsuyama, K. Tobita, M. Kaneko, and K. Nakamura, "Prediction of proximal femur strength using a CT-based nonlinear finite element method: Differences in predicted fracture load and site with changing load and boundary conditions," *Bone.* 2009 Aug; 45(2): 226-31. [PMID: 19398043]; [DOI: 10.1016/j.bone.2009.04.241]

10 S. Yano *et al.*, "Determinants of fracture type in the proximal femur: Biomechanical study of fresh frozen cadavers and finite element models," *Bone*. 2022 May; 158: 116352. [PMID: 35181576]; [DOI: 10.1016/j.bone.2022.116352]

11 M. Franceschini, L. La Barbera, A. Anticonome, C. Ottardi, A. Tanaka, and T. Villa, "Periprosthetic femoral fractures in sideways fall configuration: comparative numerical analysis of the influence of femoral stem design," *HIP Int.*, 2020 Dec; 30(2_suppl): 86-93. [PMID: 33267694]; [DOI: 10.1177/1120700020971312]

12 D. Chalhoub *et al.*, "Areal and volumetric bone mineral density and risk of multiple types of fracture in older men," *Bone*, 2016 Nov; 92: 100-106. [PMID: 27554426]; [PMCID: PMC5056840]; [DOI: 10.1016/j.bone.2016.08.014]

13 A. Izmin, M. Todo, and T. Yamamoto, "Biomechanical Effects of Bone Quality and Implant Design on Femoral Damage Mechanism in Total Hip Arthroplasty," *International Journal of Orthopaedics,* 2023; 10(1): 1721-1729. [DOI: 10.17554/j.issn.2311-5106.2023.10.483].

14 J. H. Keyak, S. A. Rossi, K. A. Jones, and H. B. Skinner, "Prediction of femoral fracture load using automated finite element modeling," *J. Biomech.*, 1998 Feb; 31(2): 125-33. [PMID: 9593205]; [DOI: 10.1016/s0021-9290(97)00123-1]

15 T. S. Keller, "Predicting the compressive mechanical behavior of bone," *J. Biomech.*, 1994 Sep; 27(9): 1159-68. [PMID: 7929465]; [DOI: 10.1016/0021-9290(94)90056-6]

16 M. I. Z. Ridzwan, S. Shuib, A. Y. Hassan, A. A. Shokri, and M. N. Mohammad Ibrahim, "Problem of stress shielding and improvement to the hip implant designs: A review," *J. Med. Sci.*,

2007; 7(3): 460-467. [DOI: 10.3923/jms.2007.460.467]

17 T. M. Keaveny, E. F. Wachtel, W. C. Hayes, and C. A. Dana, Differences between the tensile and compressive strengths of bovine tibial trabecular bone depend on modulus. J Biomech. 1994 Sep;27(9):1137-46. [PMID: 7929463]; [DOI: 10.1016/0021-9290(94)90054-x]

18 T. S. Kaneko, M. R. Pejcic, J. Tehranzadeh, and J. H. Keyak, "Relationships between material properties and CT scan data of cortical bone with and without metastatic lesions," *Med. Eng. Phys.*, 2003 Jul; 25(6): 445-54. [PMID: 12787982]; [DOI: 10.1016/s1350-4533(03)00030-4]

19 L. Røhl, E. Larsen, F. Linde, A. Odgaard, and J. Jørgensen, "Tensile and compressive properties of cancellous bone," *J. Biomech.*, 1991; 24(12): 1143-9. [PMID: 1769979]; [DOI: 10.1016/0021-9290(91)90006-9]

20 Bassam A. Masri, "Periprosthetic fractures: Evaluation and Treatment," *Clin. Orthop.,* no. 420, pp. 80-95, 2004, [DOI: 10.1097/01.blo.0000122241.70546.eb]